Vectorial nonlinear dynamics in lasers with one or two stable eigenstates

Jean-Charles Cotteverte, Fabien Bretenaker,* and Albert Le Floch
Laboratoire d'Electronique Quantique—Physique des Lasers, Université de Rennes I, F-35042 Rennes Cédex, France

Pierre Glorieux
Laboratoire de Spectroscopie Hertzienne, Université de Lille I, F-59655 Villeneuve d'Ascq Cédex, France
(Received 6 October 1993; revised manuscript received 8 December 1993)

The dynamical behavior of the polarization of a laser with one or two stable eigenstates subjected to the action of an ac longitudinal magnetic field with or without a dc longitudinal magnetic field is investigatged both theoretically and experimentally. In the case of an ac magnetic field only, the low-field linear and high-field nonlinear behaviors of the laser are isolated. For the low-field case, a typical cutoff frequency due to pure cavity effects is introduced. For the high-field case, two locations of the motion are isolated, depending on the amplitude and frequency of the ac magnetic field. This provides the tools used to understand the locking between the rotation of the polarization induced by the dc magnetic field and the vibration of the polarization induced by the ac magnetic field. In particular, thanks to the two dimensions of the polarization vector, it is shown that the ratio of locked frequencies depends on the number of stable polarization eigenstates. Unlike mechanical systems where coalescence of Arnold tongues is possible, our system, without any inertia, exhibits typical twisted Arnold tongues, for which a theoretical model provides a great precision and a good agreement between theory and experiment.

PACS number(s): 42.60.Mi

I. INTRODUCTION

Much interest has recently been devoted to the dynamical behavior of *vectorial systems,* which have been shown to exhibit instabilities. Indeed, some vectorial instabilities have been observed in mechanical vectorial systems such as a compass needle [1], or a bipolar motor [2], subjected to the superposition of a dc and an ac magnetic field. In particular, these systems have exhibited frequency locking and chaos, like many scalar systems [3]. In these systems, a dc magnetic field alone fixes an equilibrium position around which a *vibrational motion* can take place. In addition, an ac or rotating magnetic field produces a *rotational motion.* Chaos can occur in these systems because inertia imposes the existence of two dynamic variables: the angular position θ of the vector and its angular velocity $\dot{\theta}$. An external forcing (the ac magnetic field) provides then the third dynamic variable necessary to obtain chaotic behavior [4]. Instabilities and chaos have also been observed on the two scalar variables of a laser, namely, its intensity [5] and its phase [6]. Some vectorial instabilities have also been observed [7,8] or theoretically predicted [9,10] with the *polarization of a laser.* In particular, in the case of a laser subjected to the Earth's magnetic field [11,12], this has recently led to the design of a new type of laser magnetometer [13]. Thus the question arises now as to whether the polarization vector of a laser can exhibit a behavior similar to that of a compass needle. The polarization vector of a laser does not have any inertia, but, in addition to its *orientation* θ, it is also defined by its *length* (the intensity of light) and its *thickness* (the ellipticity) [14], which may replace $\dot{\theta}$ as one of the three necessary dynamic variables. Moreover, both rotation and vibration motions can also be obtained with the polarization of a laser, each one at its own frequency. In a preceding paper [15], the rotational motion and the *locking* between the rotation and vibration motions have already been observed. However, in this work, as only weak amplitudes of the ac forcing could be generated, one could not investigate the possibility for the locking tongues to overlap. Here, after having exhaustively studied the vibrational motion with weak or strong amplitudes of the forcing, we will investigate whether the application of such strong ac forcings together with a dc forcing can make the locking tongues overlap, offering then the possibility of chaos. This would allow us, when the intensity is almost constant and the polarization remains linear, to consider to some extent the polarization of light as an "optical compass."

In the absence of magnetic field, the distribution of polarization in the laser cavity is fixed by the eigenstates, calculated by the resonance condition [16], i.e., the self-consistency of the light field after one round-trip in the cavity. Depending on the nature of the linear anisotropies (loss or phase), and because of the two-dimensionality of the Jones vector, *only one or both eigenstates can be stable* [17]. The aim of this paper is to study the effects of a weak or strong ac magnetic field and of the simultaneous action of an ac and a dc magnetic field on the polarization dynamics of a laser, which will appear to depend strongly on the stability of the eigenstates. The importance of the existence of one or two stable eigenstates leads us to recall the eigenstates' stability conditions (Sec. II). Following this approach, Secs. III and

*Also at Société d'Applications Générales d'Electricité et de Mécanique, 70-74, rue de la Tour-Billy, Boîte Postale 72, F-95101 Argenteuil Cédex, France.

IV are devoted to the study of the dynamical behavior of the polarization of a laser with one and two stable eigenstates, respectively. Finally, Sec. V summarizes the results and discusses some unsolved problems.

II. STABILITY OF THE EIGENSTATES OF THE UNPERTURBED LASER

As will be shown in the following, the dynamical behavior of a forced system strongly depends on its equilibrium state. Therefore it is interesting to first recall the results previously obtained on the stability of the two eigenstates of a laser in the absence of magnetic field. The experimental system here is the 3.39-μm He-Ne laser operating on a $J=1\rightarrow J=2$ transition. In this case, the weak atomic coupling allows linearly polarized eigenstates to oscillate [18]. These linear eigenstates are determined by the intracavity anisotropies, and calculated thanks to the resonance condition $\mathbf{ME}=\lambda\mathbf{E}$ [16], where $\mathbf{M}$ is the 2×2 Jones matrix for one round-trip in the cavity, and $\mathbf{E}$ is the Jones vector of the laser light. To each eigenstate, there may correspond different losses and resonance frequencies. In particular, in our case of a laser containing loss and phase linear anisotropies [Fig. 1(a)], these eigenstates are perpendicularly linearly polarized. Their eigenfrequency difference is proportional to the phase anisotropy, and the difference between their net gains depends of course on the value of the loss anisotropy. Depending on the relative values of these linear loss and phase anisotropies, competition effects will allow only one or both eigenstates to be stable [17], as shown in Fig. 1(b). The typical shape of these stability domains is shown here in the plane $(t_x/t_y-1,\Delta\Phi_{xy})$. t_x/t_y is the ratio of the electric field transmission coefficients of the intracavity tilted plate that creates the loss anisotropy, and $\Delta\Phi_{xy}$ is the phase anisotropy for one pass in the intracavity stressed plate, where the x and y axes are defined in Fig. 1. The two domains are separated by a line which depends on the excitation of the active medium, and which can be calculated thanks to a third-order theory [19]. These domains are computed by considering the sign of the cross-saturated gain of each eigenstate, i.e., the gain of one eigenstate saturated by the field of the other one. The two-stable-eigenstate domain corresponds to the case where the cross-saturated gains of the two eigenstates have the same sign, either positive (vectorial simultaneity) or negative (vectorial bistability) [17]. On the contrary, in the one-stable-eigenstate domain, only one of the eigenstates always has a negative cross-saturated gain and can never oscillate. This stability analysis can also be performed in the framework of a Landau potential $V(E_x,E_y)$ model, where the electric fields E_x and E_y of the two eigenstates are taken as order parameters [20], and where the atomic variables have been adiabatically eliminated. From this point of view [see Fig. 1(b)], the one-stable-eigenstate regime corresponds to a one-well (along the lower loss axis) potential and the two-stable-eigenstate regime corresponds to a two-well potential. Notice that for the relatively weak phase anisotropies considered here, a two-stable-eigenstate regime always corresponds to vectorial bistability. Vectorial simultaneity would indeed occur for much larger values of the phase anisotropy [17]. In the following, we will study the simplest case of either a pure controlled loss anisotropy [x axis of Fig. 1(b)], leading to the stability of only one stable eigenstate, or a pure controlled phase anisotropy (y axis of Fig. 1), leading to the stability of both eigenstates. These concepts of eigenstate and of stability are valid only for our laser with no magnetic field, but they appear to be useful to understand the dynamical behavior of the laser subjected to a nonstationary magnetic field, hereafter called a forced laser.

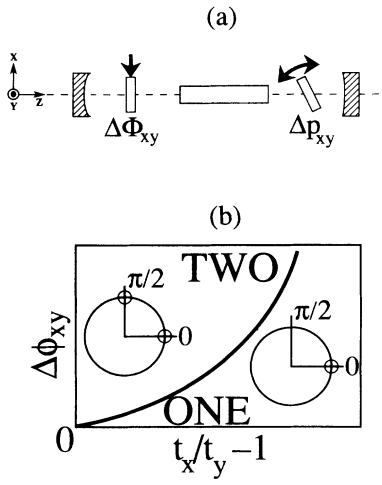

FIG. 1. (a) Laser containing loss (Δp_{xy}) and phase ($\Delta\Phi_{xy}$) anisotropies. (b) One-eigenstate and two-eigenstate stability domains. The diagram is displayed in the plane of phase anisotropies versus loss anisotropies. In each domain, the corresponding potential wells are represented. The abscissa and ordinate axes correspond to pure loss and phase anisotropies, respectively.

III. MAGNETIC FORCING OF THE ONE-STABLE-EIGENSTATE LASER

As recalled in the preceding section, when the laser of Fig. 1(a) contains only a loss anisotropy (given, e.g., by a tilted plate), it exhibits, in the absence of magnetic field, only one stable eigenstate, polarized along the x axis. Besides, it has been shown that when this laser is perturbed by a longitudinal dc magnetic field B_{dc}, its polarization exhibits a typical Adler-type dynamics [11,21]. Indeed, for magnetic fields larger than the so-called critical magnetic field, the Faraday rotation induced by this magnetic field in the active medium is sufficient to make the linear polarization rotate periodically. In other words, it is strong enough to make the polarization leave the potential well imposed by the anisotropies of the optical elements of the laser cavity. This rotation is similar to that of the compass needle subjected to a rotating (ac) magnetic field. Besides, a longitudinal ac magnetic field applied to the active medium [22] makes the sign of the Faraday rotation change periodically, and thus induces a polarization vibration similar to the vibration of the compass needle subjected to a dc magnetic field. In this section, we investigate theoretically and experimentally the behavior

of the light polarization when the one-stable-eigenstate laser is subjected first to an ac magnetic field alone and then to the simultaneous action of an ac and a dc longitudinal magnetic field, and we compare these behaviors with those of the compass needle.

A. Theoretical predictions

The one-stable-eigenstate laser with a pure loss anisotropy subjected to the superposition of a dc longitudinal magnetic field B_{dc} and an ac longitudinal magnetic field $B_{ac}\cos(\omega_{ac}t)$ can be described by the angle θ of its polarization with respect to the x axis of Fig. 1(a) and by its normalized intensity I [23] through the following differential equations:

$$\frac{d\theta}{dt}=M\sin 2\theta+\Gamma(I)[B_{dc}+B_{ac}\cos\omega_{ac}t]\ , \tag{1a}$$

$$\frac{dI}{dt}=-(K_x\cos^2\theta+K_y\sin^2\theta)I+\frac{D_0 I}{1+\zeta I}\ . \tag{1b}$$

Here K_x and K_y are the loss coefficients (positive) for the x and y polarizations, D_0 the unsaturated gain coefficient, and $\Gamma(I)$ the saturated Faraday rotation coefficient which depends on the intensity. The saturation of the gain coefficient D_0 is taken into account by the factor $1/(1+\zeta I)$, where ζ depends on the degree of homogeneity of the transition. In particular, for a homogeneous transition, one must take $\zeta=1$ while for an inhomogeneous transition one must take $\zeta=0.5$ (we consider only low intensity levels). For intermediate cases, taking a value of ζ between 0.5 and 1 will give a convenient approximation of the saturation behavior of the transition. $M<0$ is defined by

$$M=\frac{c}{2L}\left[1-\frac{t_x}{t_y}\right]\ , \tag{2}$$

where t_x and t_y are the electric field transmission coefficients of the tilted plate which creates the loss anisotropy, for the x and y polarizations, respectively. c is the velocity of light, and L the cavity length. In these equations, we have adiabatically eliminated the atomic variables, which are much more rapid than the field variables. Besides, as we consider only a pure loss anisotropy, we can regard the polarization as a linear polarization at angle θ, without any ellipticity. In the absence of any magnetic field, Eq. (1a) leads then to a stable equilibrium position at $\theta=0$, and an unstable equilibrium position at $\theta=\pi/2$, which correspond, respectively, to the well and the saddle point of the potential discussed in Sec. II. Equation (1b) describes the variations of the laser intensity I due to the different losses undergone by the laser when θ passes from the lower loss axis x to the higher loss axis y. However, we restrict ourselves to the case of weak loss anisotropies ($t_x/t_y-1\ll 1$) and $1/D_0$ is short compared to the typical time scales of the system, allowing us to consider I as constant and to eliminate it adiabatically. Equations (1) then simply reduce to the following forced Adler-type equation:

$$\frac{d\theta}{dt}=M\sin 2\theta+\gamma(B_{dc}+B_{ac}\cos\omega_{ac}t)\ , \tag{3}$$

where γ is now the saturated Faraday rotation coefficient. If $B_{ac}=0$, there is not any forcing anymore, but only the dc magnetic field B_{dc}. Then, θ evolves monotonically if B_{dc} is larger than the critical field $B_c=M/\gamma$, and the signal observed through a polarizer has an angular frequency $\omega_{dc}=2\gamma B_{dc}(1-B_c^2/B_{dc}^2)^{1/2}$. As stated above, we will begin with $B_{dc}=0$.

1. $B_{dc}=0$: *Pure vibration dynamics*

Starting from the laser at rest in its stable eigenstate, in the case of small sinusoidal magnetic perturbations, Eq. (3) may be linearized, and we can discuss the frequency response of the linearized system. The nonlinear behavior of the system subjected to large magnetic fields is treated in the following subsection.

(a) Small amplitude motions around $\theta=0$. In the case where the alternative field amplitude B_{ac} is small compared to M/γ, θ will remain around 0, and then Eq. (3) can be linearized with respect to θ, to read

$$\frac{d\theta}{dt}=2M\theta+\gamma B_{ac}\cos\omega_{ac}t\ . \tag{4}$$

For the sake of simplicity, we assume the origin at the equilibrium state. This linear first-order differential equation leads, in the permanent regime, to a sinusoidal time evolution of θ around the stable position $\theta=0$ at angular frequency ω_{ac} with an amplitude Θ_1 and phase φ_1 given by

$$\theta(t)=\Theta_1\sin(\omega_{ac}t+\varphi_1)\ , \tag{5a}$$

$$\Theta_1=\frac{\gamma B_{ac}}{\sqrt{\omega_{c1}^2+\omega_{ac}^2}}\ , \tag{5b}$$

$$\varphi_1=-\arctan(\omega_{c1}/\omega_{ac})\ , \tag{5c}$$

where

$$\omega_{c1}=\frac{c}{L}\left[\frac{t_x}{t_y}-1\right] \tag{6}$$

is the $1/\sqrt{2}$ cutoff angular frequency of the polarization in the case of a loss anisotropy, which limits the bandwidth of the modulation. This means that for a given B_{ac}, the amplitude Θ_1 of the movement of θ is $\sqrt{2}$ smaller for $\omega_{ac}=\omega_{c1}$ than for $\omega_{ac}\ll\omega_{c1}$. In the experiment, we will measure the laser output power $P(t)$ through a polarizer:

$$P(t)=P_0\cos^2[\theta(t)-\theta_p]\ , \tag{7}$$

where θ_p is the angle between the axis of the polarizer and the x axis. Equation (7) then becomes

$$P(t)=\frac{P_0}{2}\{1+\cos[2\Theta_1\sin(\omega_{ac}t+\varphi_1)-2\theta_p]\}\ . \tag{8}$$

Thanks to a Bessel function expansion [24], we obtain

$$P(t)=\frac{P_0}{2}\left[1+\cos 2\theta_p\left[J_0(2\Theta_1)+2\sum_{n=1}^{\infty}J_{2n}(2\Theta_1)\cos 2n(\omega_{ac}t+\varphi_1)\right]\right]$$
$$+\frac{P_0}{2}\left[\sin 2\theta_p\left[2\sum_{n=0}^{\infty}J_{2n+1}(2\Theta_1)\sin(2n+1)(\omega_{ac}t+\varphi_1)\right]\right]. \quad (9)$$

As already observed by Culshaw and Kannelaud [22], Eq. (9) shows that odd harmonics of ω_{ac} vanish when the axis of the polarizer is oriented along one of the eigenstates ($\theta_p=0$ or $\pi/2$), and even harmonics disappear when the axis of the polarizer is aligned along one of the bisectors of x and y ($\theta_p=\pi/4$ or $3\pi/4$). However, these authors considered the response of the polarization to the ac magnetic field to be instantaneous. This would be valid only for a single pass of light through a Faraday medium, for which the orientation of the output polarization would be exactly proportional to the weak magnetic field. For a weak ac Faraday rotation occurring inside a cavity, we must consider a differential equation, because the light goes alternatively through the active medium and the anisotropies. Indeed, because of the cumulative nature of the Faraday rotation, the back and forth propagation inside the cavity makes the response of the polarization to the ac magnetic field variations slower. But, the accumulation of the Faraday rotation, thanks to the multiple passes in the Faraday medium, provides a larger amplitude of vibration of the polarization than for a single pass. The cutoff frequency of Eq. (6) resulting from these cavity effects can be seen from the full line of Fig. 2, which displays the typical theoretical evolution of the predominant component $J_1(2\Theta_1)$ of $P(t)$ at ω_{ac} versus modulation frequency.

(b) Large amplitude motions. When B_{ac} becomes large compared to M/γ, the polarization leaves the potential well and makes several turns in one direction during a given half period of the ac forcing. We notice from Eq. (3) that for $B_{ac}\gg M/\gamma$, the locking term $M\sin 2\theta$ is most of the time small compared to the forcing term $B_{ac}\cos(\omega_{ac}t)$. Consequently, we look for a solution of

$$\frac{d\theta}{dt}=M\sin 2\theta+\gamma B_{ac}\cos\omega_{ac}t\ , \quad (10)$$

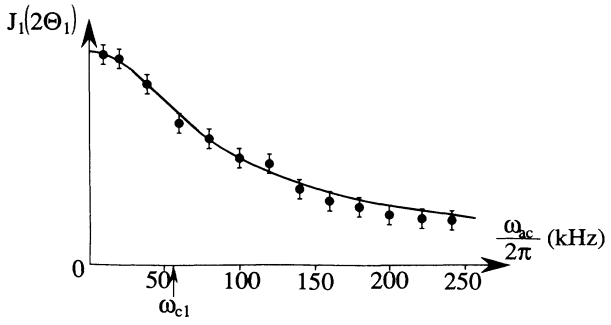

FIG. 2. Response of the polarization to an ac magnetic field in the case of one stable eigenstate. $J_1(2\Theta_1)$, proportional to the modulation of the intensity observed through the polarizer, is represented versus the frequency of the ac magnetic field (full line: theory; dots: experiment).

of the shape

$$\theta(t)=\frac{\gamma B_{ac}}{\omega_{ac}}\sin\omega_{ac}t+\theta_0(t)\ , \quad (11)$$

in which the leading term has been made explicit. θ_0 is smaller than the leading term amplitude $\gamma B_{ac}/\omega_{ac}$. After a time averaging over one period of the forcing frequency, we keep only the slowest varying term and obtain

$$\langle\dot{\theta}_0\rangle=MJ_0\left[\frac{2\gamma B_{ac}}{\omega_{ac}}\right]\sin(2\theta_0)\ . \quad (12)$$

This equation for θ_0 has the same shape as Eq. (10) for θ, with the locking term just multiplied by $J_0(2\gamma B_{ac}/\omega_{ac})$. It leads to two "equilibrium" values for θ_0: $\theta_0=0$ and $\pi/2$. Depending on the sign of the new locking coefficient $\bar{M}=MJ_0(2\gamma B_{ac}/\omega_{ac})$, either one solution or the other is stable. As $M<0$, $\theta_0=0$ is stable for $J_0(2\gamma B_{ac}/\omega_{ac})>0$ and $\theta_0=\pi/2$ is stable for $J_0(2\gamma B_{ac}/\omega_{ac})<0$. For the large values of B_{ac} considered here, we have

$$\bar{M}\approx M\left[\frac{\omega_{ac}}{\pi\gamma B_{ac}}\right]^{1/2}\cos\left[\frac{2\gamma B_{ac}}{\omega_{ac}}-\frac{\pi}{4}\right], \quad (13)$$

and the motion of θ will take place around 0 for $2p\pi-\pi/4<2\gamma B_{ac}/\omega_{ac}<2p\pi+3\pi/4$ and around $\pi/2$ for $2p\pi+3\pi/4<2\gamma B_{ac}/\omega_{ac}<2p\pi+7\pi/4$, p being an integer. In particular, the values $2\gamma B_{ac}/\omega_{ac}=p\pi+3\pi/4$ will correspond to a transition for the mean position of the polarization. Then, for large amplitude motions, the mean value of θ, around which the motion occurs, can only take two values, which correspond to the stable and the unstable eigenstates. The motion's mean value will flip between the two eigenstates, for particular values of $2\gamma B_{ac}/\omega_{ac}$. Then, for each B_{ac}, there exists a set of values of ω_{ac} given by $\omega_{ac}=2\gamma B_{ac}/(p\pi+3\pi/4)$, for which the mean value of the polarization flips from one eigenstate to the other. This behavior can also be understood in terms of potential wells (see Fig. 3). Because of considerations of symmetry (the potential is symmetrical around the stable eigenstate, $\theta_0=0$, and around the unstable eigenstate, $\theta_0=\pi/2$), the motion must take place around either $\theta_0=0$ or $\theta_0=\pi/2$. The choice between $\theta_0=0$ and $\theta_0=\pi/2$ depends on the slope of the potential at the U turns of the motion. Indeed, one can see from (11) and (12) that θ_0 is chosen so that the U turns occur along the "natural" slope of the potential, i.e., that the system climbs the barrier before each U turn, and slides back down the barrier after the U turn. Depending on the value of $2\gamma B_{ac}/\omega_{ac}$, this fixes the position of θ_0. For example, in Fig. 3(a) [respectively, 3(b)], the amplitude of the movement obliges the oscillation to be centered

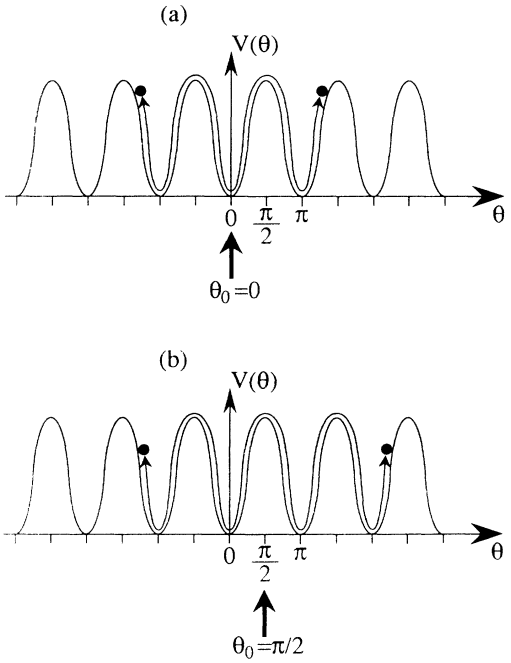

FIG. 3. Schematic representation of the evolution of θ in the potential V when the one-stable-eigenstate laser is submitted to a strong ac magnetic field alone. For the U turns to occur along the natural slope of the potential, the movement must be centered around either $\theta_0=0$ (a) or $\theta_0=\pi/2$ (b), depending on the values of B_{ac} and ω_{ac}. The big dots show the positions of the U turns in both cases.

around $\theta_0=0$ (respectively, $\theta_0=\pi/2$), so that the U turns occur along the "natural slope" of the potential.

We have only considered here the limit cases of a weak or a strong ac magnetic field. For intermediate values of B_{ac}, the polarization barely leaves its potential well.

2. *Superimposed ac and dc magnetic fields*

In this case, an ac and a dc magnetic field are simultaneously applied, inducing a vibrational motion and a rotational motion, respectively. Because of the nonlinear term in Eq. (3), locking effects between vibration and rotation frequencies are expected to occur. This part will be devoted to the analytical study of these locking effects on the one hand, and their physical understanding on the other.

Let us first explain physically the locking phenomenon between rotational and vibrational motions. In the preceding sections, we have seen that static and alternating magnetic fields induce rotation at angular frequency ω_{dc} and vibration at angular frequency ω_{ac}, respectively. Locking occurs when the combination of these two motions results in a single periodic motion at angular frequency ω_{ac} while in the general case of unlocking, these two motions coexist and are more or less independent. In the phase space, unlocked vibration and rotation correspond to motion on a torus while the locked states are represented by limit cycles. In linear systems, these two motions are uncoupled, but here nonlinearity is responsible for the locking. Because of this origin, locking occurs more easily as the driving terms are large and/or when the two frequencies which lock are commensurate. In our case, this would correspond to $\omega_{ac}/p=\omega_{dc}/q$. However, we will first see why here ω_{dc}/n locks only with ω_{ac}, and secondly why there are some values of B_{ac} which make the locking range maximum and some others which make the locking range null. To do this, we adopt the point of view followed by Rocard [25] for classical oscillators, who considered the locking between free and forced oscillations to be strong or weak depending on the matching between these two oscillations. In the same way, Fig. 4 depicts the locking between ω_{ac} and ω_{dc}/n. Figure 4(a) represents the time evolution of θ, i.e., pure rotation, with only the dc magnetic field. The evolution is not linear because of the anisotropies. Figures 4(b)–4(d) represent the time evolution of θ with only the ac magnetic field, for three different values of ω_{ac}, submultiple of ω_{dc}. We notice that for those three particular values, θ passes through 0 at the same time and with the same direction as for the dc magnetic field alone. Then, the lockings follow the law $\omega_{ac}\approx\omega_{dc}/n$. In Fig. 4, only a weak ac magnetic field was considered. When its amplitude is larger, i.e., sufficient to make the polarization leave the potential well when the ac magnetic field is applied alone, other effects arise. Because the total magnetic field is most of the time larger than the critical magnetic field, ω_{ac} will lock with $2\gamma B_{dc}$ instead of $\omega_{dc}=2\gamma B_{dc}(1-B_c^2/B_{dc}^2)^{1/2}$ with $B_c=M/\gamma$. ω_{dc} is close to $2\gamma B_{dc}$ instead of γB_{dc} because θ and $\theta+\pi$ are physically equivalent and indistinguishable through a polarizer. Figure 5 then shows the evolution of θ when a dc magnetic field and a strong ac magnetic field are applied, when $\omega_{ac}=2\gamma B_{dc}$, and when $\omega_{ac}>2\gamma B_{dc}$. In this latter

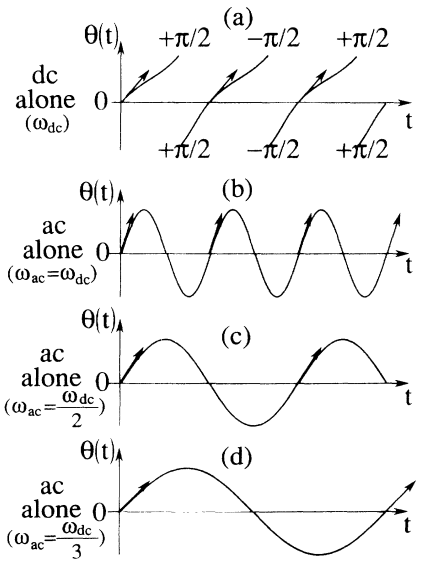

FIG. 4. Physical understanding of the locking law $\omega_{ac}\approx\omega_{dc}/n$ in the case of one stable eigenstate. (a) is the time evolution of θ (at pulsation ω_{dc}) with only the dc magnetic field. (b), (c), and (d) are the time evolutions of θ when only a weak ac magnetic field is applied, at three different pulsations ω_{ac}, submultiples of ω_{dc}.

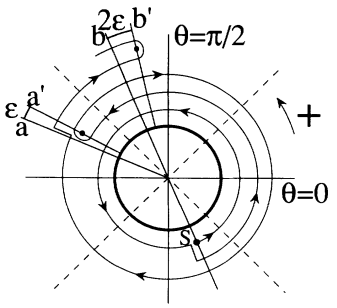

FIG. 5. Evolution of the orientation angle θ of the polarization during one period of the ac magnetic field when the dc and ac magnetic fields are applied simultaneously. Starting from S and neglecting the nonlinear term, the next U turn occurs at point a if $\omega_{ac}=2\gamma B_{dc}$, or at point a' if $\omega_{ac}>2\gamma B_{dc}$, after one half period of the ac magnetic field. After the following half period, the U turns occur, respectively, at points b and b'. The role of the nonlinearity is to bring a' and b' back to a and b, i.e., to compensate for the delay ε, and thus to maintain the locking between the rotational and vibrational motions.

case, an angular shift ε occurs at each U turn. ε is the difference, for one half period of the ac magnetic field, between a nonlinear time evolution of θ (caused by the anisotropy), and a linear time evolution. Using a calculation performed by Chow *et al.* [26] for locking in laser gyros, the nonlinear evolution of θ can be written as

$$\theta_{NL}(t)=\theta_L(t)+\delta(t) , \tag{14}$$

where $\theta_L(t)$ is the time evolution of θ, in the case where nonlinearity is neglected ($M=0$):

$$\theta_L(t)=\gamma B_{dc}t+\frac{\gamma B_{ac}}{\omega_{ac}}\sin(\omega_{ac}t) . \tag{15}$$

In Eq. (14), δ is the nonlinear contribution of the anisotropy to the time evolution of θ, and makes the polarization behave as if $\omega_{ac}=2\gamma B_{dc}$, although $\omega_{ac}>2\gamma B_{dc}$. ε is then the opposite of the variation of δ for one half period of the ac magnetic field, i.e., between two successive U turns of the polarization. By reintroducing (14) in (3), we obtain

$$\dot{\delta}(t)=M\sin\left[2\gamma B_{dc}t+\frac{2\gamma B_{ac}}{\omega_{ac}}\sin\omega_{ac}t+2\delta(t)\right] . \tag{16}$$

Expanding in terms of Bessel functions yields

$$\dot{\delta}(t)=\sum_{m=-\infty}^{+\infty} MJ_m\left[\frac{2\gamma B_{ac}}{\omega_{ac}}\right] \times\sin[(2\gamma B_{dc}+m\omega_{ac})t+2\delta(t)] , \tag{17}$$

where J_m is the Bessel function of order m. We are interested in locking between ω_{ac} and $2\gamma B_{dc}$. Because of time averaging effects, only the slowly varying resonant term survives, simplifying Eq. (17) significantly:

$$\dot{\delta}(t)\approx MJ_{-1}\left[\frac{2\gamma B_{ac}}{\omega_{ac}}\right]\sin[(2\gamma B_{dc}-\omega_{ac})t+2\delta(t)] . \tag{18}$$

This can be brought into a more familiar form, thanks to the substitution

$$\varphi(t)=(2\gamma B_{dc}-\omega_{ac})t+2\delta(t) . \tag{19}$$

We then obtain

$$\dot{\varphi}(t)=2\gamma B_{dc}-\omega_{ac}+2MJ_{-1}\left[\frac{2\gamma B_{ac}}{\omega_{ac}}\right]\sin[\varphi(t)] . \tag{20}$$

This equation is again an Adler-type equation [21]. Locking occurs when $\dot{\varphi}(t)=0$, i.e., when δ compensates the shift symbolized by ε in Fig. 5. Introducing ε in Eq. (19) yields

$$\varphi(t)=2\delta(t)-\frac{\varepsilon\omega_{ac}}{\pi}t . \tag{21}$$

Thus $\varphi(t)$ behaves as an error signal, in order to maintain the locking between ω_{ac} and $2\gamma B_{dc}$. If $J_{-1}(2\gamma B_{ac}/\omega_{ac})\neq 0$, $\varphi(t)$ can first drift, until the slope of $\sin\varphi(t)$ is such that $\dot{\varphi}(t)=0$, which corresponds to a locked state. But, if $J_{-1}(2\gamma B_{ac}/\omega_{ac})=0$, $\dot{\varphi}(t)$ cannot be null if $\omega_{ac}\neq 2\gamma B_{dc}$. No locking can then occur. To extract the locking zones, $\dot{\varphi}(t)=0$ leads to

$$0\leq\left|\frac{2\gamma B_{dc}-\omega_{ac}}{2MJ_{-1}\left[\frac{2\gamma B_{ac}}{\omega_{ac}}\right]}\right|\leq+1 . \tag{22}$$

The locking tongues, for the general case where ω_{ac} and $2\gamma B_{dc}/n$ are locked, are then limited by these two curves in the plane $(\omega_{ac}/2\pi, B_{ac})$, for a fixed B_{dc}:

$$\omega_{ac}=\frac{2\gamma B_{dc}}{n}-\frac{2M}{n}J_{-n}\left[\frac{2\gamma B_{ac}}{\omega_{ac}}\right] , \tag{23a}$$

$$\omega_{ac}=\frac{2\gamma B_{dc}}{n}+\frac{2M}{n}J_{-n}\left[\frac{2\gamma B_{ac}}{\omega_{ac}}\right] . \tag{23b}$$

They are represented in Fig. 6 for a fixed value of B_{dc}, and for three different values of n. Note that ω_{ac} does not lock with ω_{dc}/n exactly, but with $2\gamma B_{dc}/n$, a value which would be equal to ω_{dc}/n if there was no anisotro-

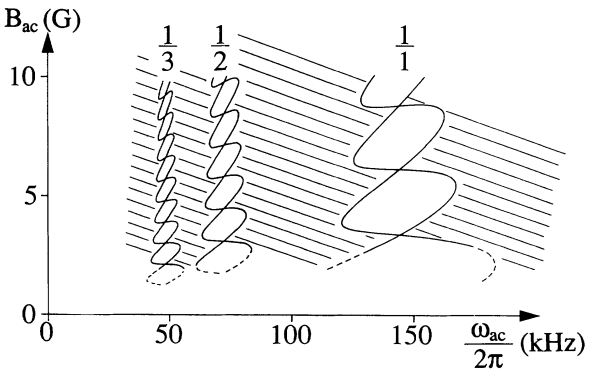

FIG. 6. Theoretical locking tongues obtained analytically from Eqs. (23), valid only for a rather high amplitude of the ac magnetic field. The hatched domains correspond to a motion with unlocked frequencies (quasiperiodicity).

py. This is due to the fact that the total magnetic field $B_{dc}+B_{ac}\cos(\omega_{ac}t)$ is most of the time much greater than the critical field, so that the anisotropies are rarely influential. Moreover, one can find values of B_{ac} for which locking is less efficient, i.e., for which the width of the locking tongue is null, by equalizing Eqs. (23). This condition leads to

$$J_{-n}\left[\frac{2\gamma B_{ac}}{\omega_{ac}}\right]=0 . \tag{24}$$

The roots of (24) give the values of B_{ac} for which the range of $\omega_{ac}/2\pi$ where locking occurs is null. Between these roots, there are some values for which this range is maximum. For sufficiently high values of B_{ac}, (24) can be approximated by

$$\left[\frac{\omega_{ac}}{\pi\gamma B_{ac}}\right]^{1/2}\cos\left[\frac{2\gamma B_{ac}}{\omega_{ac}}-n\frac{\pi}{2}-\frac{\pi}{4}\right]=0 . \tag{25}$$

For example, for $n=1$ ($\omega_{dc}\approx\omega_{ac}$), the locking range of $\omega_{ac}/2\pi$ will be null for $2\gamma B_{ac}/\omega_{ac}=\pi/4+k\pi$, and maximum for $2\gamma B_{ac}/\omega_{ac}=3\pi/4+k\pi$, k being an integer.

We have obtained *twisted Arnold tongues* (see Fig. 6), characterized by the fact that their widths vary with B_{ac} and with M, and that they do not overlap, ruling out the possibility of chaos by the quasiperiodicity route [3]. Three dynamic variables are indeed necessary to observe chaos: we only have θ and the forcing $\gamma B_{ac}\cos\omega_{ac}t$, because I is adiabatically eliminated.

B. Experimental verification for one stable eigenstate

The experimental scheme is displayed in Fig. 7. The cavity is 54.5 cm long. In order to choose between loss anisotropies ($t_x\neq t_y$) and phase anisotropies $\Delta\Phi_{xy}$, two silica plates are introduced inside the cavity. Plate 1 can be tilted to produce a loss anisotropy, and plate 2 can be stressed to produce a phase anisotropy (in this section, we do not use the phase anisotropy: $\Delta\Phi_{xy}=0$). The discharge tube is 18 cm long, with a 4 mm inner diameter. It is filled with a 7:1 ^{3}He-^{20}Ne mixture at a total pressure of 1.1 Torr. Mirror M_1 has a radius of curvature of 60 cm and transmits 36% of the incident light. Mirror M_2 has a radius of curvature of 6 m, transmits 5% of the incident light, and is mounted on a piezoelectric transducer. The laser oscillates at $\lambda=3.39$ μm on the usual $J=1\rightarrow J=2$ line. The weak atomic coupling of this line permits both σ components to oscillate simultaneously, and then to produce a linear polarization. The cavity is longitudinally monomode, and an aperture selects the TEM_{00} fundamental mode. Because of the extreme sensitivity of this device, great care has been taken to protect the laser from mechanical vibrations: The entire experiment is mounted on a 10-ton concrete table, resting on tire tubes. To avoid spurious reflections, the windows closing the discharge tube are tilted at calculated skew angles (2.4°) to make the residual anisotropies as weak as possible, taking the interferences between the successive reflections that occur inside the window for our given Gaussian beam into account [27]. Both mirror rests are linked with quartz rods to reduce residual drifts of the cavity length. The effects of the Earth's magnetic field have been eliminated by orienting our laser along the east-west direction [11]. The residual magnetic fields have been compensated by applying an opposite magnetic field on the discharge tube. ac and dc magnetic fields are applied with a HP 3314 wave generator, whose output is sent to a homemade amplifier, which allows us to reach an amplitude of the ac magnetic field as high as 10 G. This amplifier has a quasiflat gain in the range 0–600 kHz. The signal can be sampled with a homemade sample/hold module, triggered by the output of the generator at frequency $\omega_{ac}/2\pi$. In the following, when experimental results are compared with theoretical results or simulations, all the parameters used will be obtained from measurements, except the values of the anisotropies which are adjusted.

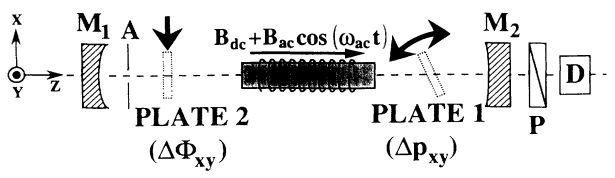

FIG. 7. Experimental setup used to observe the behavior of the polarization with an ac magnetic field alone ($B_{dc}=0$), or superimposed onto a dc magnetic field. Plate 1 produces the loss anisotropy used in the case of only one stable eigenstate, and plate 2 produces the phase anisotropy used in the case of two stable eigenstates.

1. *ac magnetic field alone*

(a) Weak ac magnetic field alone. The response of the polarization to the weak ac magnetic field alone is studied by monitoring the ac component of the intensity transmitted through a polarizer oriented at $\theta_p=45°$ versus the frequency of the ac magnetic field. The theoretical curve (full line of Fig. 2) is computed from (5), with $t_x/t_y-1=0.65\times10^{-3}$, and the dots are the experimental points. The weak amplitude of the ac magnetic field is $B_{ac}=0.1$ G. Thus the measured cutoff frequency is $\omega_{c1}/2\pi=57$ kHz. This is a first-order response, depending on the strength of the loss anisotropies, and this result is valid only for weak amplitudes of the ac magnetic field.

(b) Strong ac magnetic field alone. If the ac field is strong enough, the polarization can leave the potential well. The motion is generally $2\pi/\omega_{ac}$ periodical, either around $\theta_0=0$ or $\pi/2$, depending on the amplitude of the ac field, as discussed in case (b) of Sec. III A 1. But, for particular values of ω_{ac}, a hesitation between these two values occurs (see Fig. 8). These hesitations correspond to the predicted flips of the mean position of the polarization, and the corresponding values of $\omega_{ac}/2\pi=\gamma B_{ac}/\pi^2(p+\frac{3}{4})$ (see case (b) of Sec. III A 1) are calculated for different values of p, with $B_{ac}=5.5$ G and $\gamma=562\,000$ rad s^{-1}. We monitor this dynamical behavior by sampling the signal at $\omega_{ac}/2\pi$, then a line is obtained

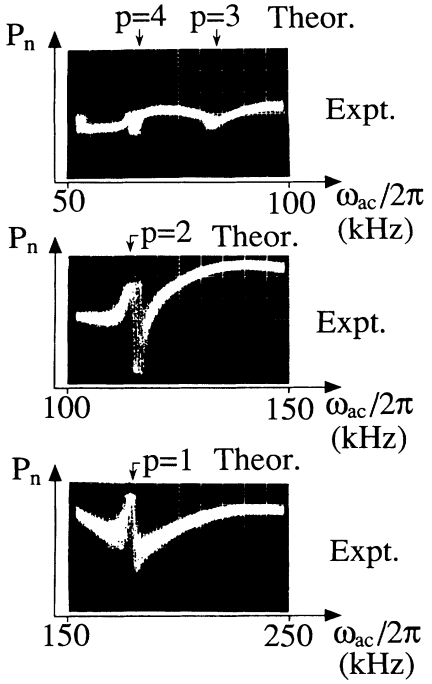

FIG. 8. Experimental signal sampled at $\omega_{ac}/2\pi$ for several values of p. Between the T_{ac}-periodical zones where θ_0 is stable, some nonperiodical zones exist, where the system hesitates between $\theta_0=0$ and $\pi/2$.

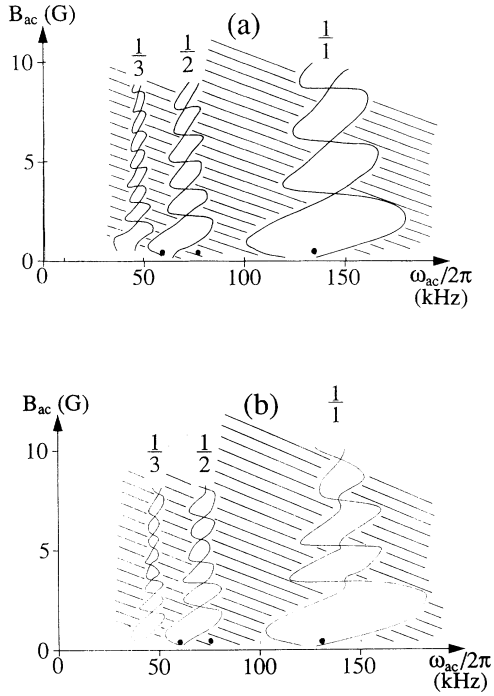

FIG. 9. Theoretical (a) and experimental (b) locking tongues in the plane $(\omega_{ac}/2\pi, B_{ac})$ for one stable eigenstate. Theoretical locking tongues (a) are obtained by simulating Eqs. (1). The hatched domains correspond to a motion with unlocked frequencies (quasiperiodicity). Dots show the location of the spectra in Fig. 11.

for the $2\pi/\omega_{ac}$-periodical signal predicted in Eqs. (11) and (12) of the preceding section, and a scrambled zone is obtained for a hesitation, in agreement with the predictions of case (b) of Sec. III A 1. This hesitation is a commutation scrambled by the residual technical noise, in spite of the great care taken to protect the experiment.

2. *Superimposed ac and dc magnetic fields*

The same experimental setup is used except that an extra longitudinal dc magnetic field $B_{dc}=0.86$ G is applied to the discharge tube. Figure 9 displays the theoretical locking tongues [Fig. 9(a)] and the experimental ones [Fig. 9(b)]. The unlocked regions between the tongues are hatched. Figure 9(a) is obtained by simulating Eqs. (1) with $t_x/t_y-1=0.8\times10^{-3}$, $\Gamma_0=1.14\times10^6$ rad $s^{-1}G^{-1}$, $K_x=110.14\times10^6$ s^{-1}, $K_y=110.61\times10^6$ s^{-1}, $D_0=240\times10^6$ s^{-1}, and $L=0.545$ m. This confirms the validity of the analytical calculation leading to Eqs. (23) (see Fig. 6). Moreover, the experimental locking tongues in Fig. 9(b) fit very well the theoretical ones. Only the locking tongues $\omega_{ac}\approx\omega_{dc}/n$ with $n\leq3$ are represented, but other tongues also exist for very low ω_{ac} (large values of n). When ω_{dc}/n and ω_{ac} are locked together, the period of the signal is $T_{ac}=2\pi/\omega_{ac}$. But when they are unlocked, the signal is no longer periodic. This is the so-called "quasiperiodic regime," although there are only the variable θ and the forcing to be involved in the dynamics. Indeed, the dc magnetic field makes θ evolve monotonically, and since we observe the laser output through a polarizer, we get the frequency $\omega_{dc}/2\pi$. Its combination with the frequency $\omega_{ac}/2\pi$ can then produce quasiperiodicity. The locking zones can be directly displayed by keeping B_{ac} constant and sweeping ω_{ac}. Then, the sampling (at frequency $\omega_{ac}/2\pi$) of the signal gives a well-defined line in the locked regions, and widely scattered points in the unlocked regions, as shown in Fig. 10 on the typical "bifurcation diagrams" obtained for $B_{ac}=0.3$ G. Figure 10(a) corresponds to $\theta_p=0$ and Fig. 10(b) to $\theta_p=45°$. This shows that rotating the polarizer is equivalent to shifting the instant of sampling. Studying the spectrum in locked and unlocked regions tells us which frequencies are present in the signal, as shown in Fig. 11, for $B_{ac}=0.3$ G. Figures 11(a)–11(c) are experimental, and Figs. 11(d)–11(f) are the corresponding theoretical spectra, calculated using the model [Eqs. (1)] with the parameters obtained from measurements except t_x/t_y-1, adjusted at 0.8×10^{-3}. Figure 11(a) is measured in the locking tongue $\frac{1}{2}$ at $\omega_{ac}/2\pi=60$ kHz. Only $\omega_{ac}/2\pi$ and its harmonics are present. Figure 11(b) corresponds to the quasiperiodic regime, where $\omega_{ac}/2\pi=75$ kHz, $\omega_{dc}/2\pi=130$ kHz, and the linear combinations of their harmonics are present. In the locking tongue $\frac{1}{1}$, Fig. 11(c) shows $\omega_{ac}/2\pi=130$ kHz and its harmonics.

With a one-stable-eigenstate laser, a typical dynamics with $1/n$ *lockings* is observed. Although lockings between rotational and vibrational motions also occur with a compass needle, *no chaos* is observed in our case, because of the adiabatic elimination of one variable, name-

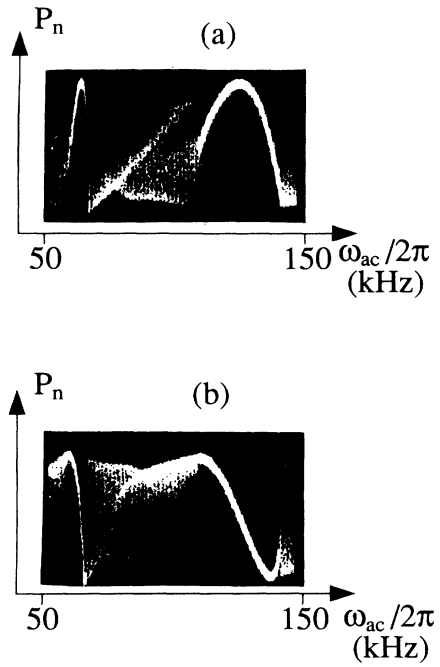

FIG. 10. Experimental bifurcation diagrams for one stable eigenstate, and for two different positions of the polarizer: (a) $\theta_p=0$; (b) $\theta_p=45°$. $B_{ac}=0.3$ G.

ly, the intensity, which reduces the number of dynamic variables. However, a typical cutoff frequency is introduced for a weak ac magnetic field alone. For a large ac magnetic field alone, the motion of the polarization is shown to occur *about the stable* ($\theta=0$) or the *unstable* ($\theta=\pi/2$) position, depending on the value of $2\gamma B_{ac}/\omega_{ac}$. With the simultaneous action of an ac and a dc magnetic field, the $1/n$ lockings occur inside typical *twisted Arnold tongues.* Good agreement is observed between theory and experiment, the locking phenomena are well understood, and the twisted Arnold tongues have been obtained for many narrowings.

Consequently, we have shown the existence of similarities between our vectorial laser and the compass needle,

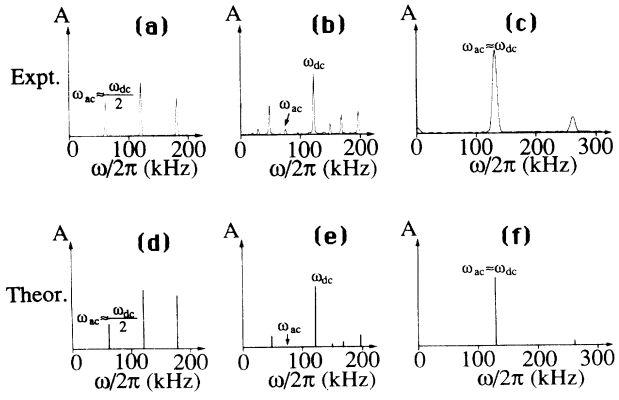

FIG. 11. Experimental (a)–(c) and theoretical (d)–(f) spectra of the signal at three different points in the plane $(\omega_{ac}/2\pi, B_{ac})$ of Fig. 8. $B_{ac}=0.3$ G. (a),(d) $\omega_{ac}/2\pi=60$ kHz; (b),(e) $\omega_{ac}/2\pi=75$ kHz; (c),(f) $\omega_{ac}/2\pi=130$ kHz.

namely, the existence of lockings between rotational and vibrational motions, and of one stable equilibrium position and one unstable equilibrium position. But, unlike in the case of the compass needle, the superposition of these two motions does not lead to chaos in the case of the polarization of the laser. This is due to the fact that the forced vectorial laser does not possess three dynamic variables, as does the compass needle.

IV. MAGNETIC FORCING OF THE TWO-STABLE-EIGENSTATE LASER

We now ask the question as to whether the ellipticity introduced by a phase anisotropy can play the role of a third dynamic variable.

When a laser contains a pure phase anisotropy in its cavity [vertical axis of Fig. 1(b)], both eigenstates are stable, either in a bistability regime, or in a simultaneity regime. In our case, they will be bistable, because the considered phase anisotropies are relatively weak, allowing the polarization to rotate thanks to the Faraday rotation.

A. Theoretical predictions

Since the loss anisotropy has been removed, the intensity is independent of the polarization and remains constant. But the phase anisotropy produces a phase shift between the two axes of the plate, and then makes the polarization elliptical. To describe the time evolution of the orientation angle and ellipticity of the polarization, we use Van Haeringen's equations [28], in which forcing terms have been added:

$$\frac{d\theta}{dt}=\left[k_d-\frac{c}{L}\Delta\phi_{xy}\cos(2\theta)\right]\chi+\gamma(B_{dc}+B_{ac}\cos\omega_{ac}t)\ , \tag{26a}$$

$$\frac{d\chi}{dt}=\frac{c}{2L}\Delta\phi_{xy}\sin(2\theta)-a\chi\ , \tag{26b}$$

where $\chi=\arctan(E_m/E_M)$ is the ellipticity of the polarization. Notice that the evolution of θ and χ has been described in other works [29]. Here, E_m and E_M are the electric field amplitudes along the minor and major axes, respectively. The coefficients k_d and a depend on the total angular momenta of the laser line and on the excitation. Their expressions can be obtained from the Lamb coefficients describing the competition between the σ^+ and σ^- components of the laser light [28]. $\Delta\Phi_{xy}$ is the phase shift between the x and y polarizations for one pass in the cavity. The eigenstates, now both stable, are still located at $\theta=0$ and $\pi/2$. Under certain approximations, Eqs. (26) can be studied analytically but, in the general case, we will have to perform simulations.

1. *ac magnetic field alone*

We now study analytically the case of the laser submitted to a weak ac magnetic field alone. Let us linearize Eqs. (26) around $\theta=0$. We obtain

$$\frac{d\theta}{dt}=\left[k_d-\frac{c}{L}\Delta\phi_{xy}\right]\chi+\gamma B_{ac}\cos\omega_{ac}t\ , \tag{27a}$$

$$\frac{d\chi}{dt}=\frac{c}{L}\Delta\phi_{xy}\theta-a\chi\ . \tag{27b}$$

In the case where the laser is tuned at line center, $k_d=0$ and Eqs. (27) yield (this assumption does not affect the generality of the result)

$$\frac{d^2\theta}{dt^2}+a\frac{d\theta}{dt}+\left[\frac{c}{L}\Delta\phi_{xy}\right]^2\theta=\gamma B_{ac}\sqrt{a^2+\omega_{ac}^2}\cos(\omega_{ac}t+\psi)\ , \tag{28}$$

where

$$\tan\psi=\frac{\omega_{ac}}{a}\ . \tag{29}$$

The amplitude of the solution of (28) is then

$$\Theta_2=\gamma B_{ac}\left[\frac{1+\left[\frac{\omega_{ac}}{a}\right]^2}{\left[\frac{\omega_{ac}^2}{a}-\frac{\left[\frac{c}{L}\Delta\phi_{xy}\right]^2}{a}\right]^2+\omega_{ac}^2}\right]^{1/2}\ . \tag{30}$$

As in our experiment ω_{ac} verifies $\omega_{ac}\ll a$ and $\omega_{ac}\ll(c/L)\Delta\phi_{xy}$, (30) leads to

$$\Theta_2=\frac{\gamma B_{ac}}{\sqrt{\omega_{c2}^2+\omega_{ac}^2}}\ , \tag{31}$$

where

$$\omega_{c2}=\frac{[(c/L)\Delta\phi_{xy}]^2}{a} \tag{32}$$

is the $1/\sqrt{2}$ cutoff frequency of the polarization in the case of phase anisotropy. The damping coefficient

$$\delta_d=\frac{a}{2(c/L)\Delta\phi_{xy}} \tag{33}$$

is strong ($\delta_d>1$) because a is large compared to $(c/L)\Delta\Phi_{xy}$ [28]. Thus the dynamics is almost first order as verified theoretically in the full line in Fig. 12, as in the case of one stable eigenstate. But, in addition, the vibrations induced by the ac magnetic field alone can take place around any of the two stable eigenstates, depending on the initial conditions.

2. *Superimposed ac and dc magnetic fields*

In this case, the addition of a vibrational motion and a rotational motion will again produce some lockings. But as both eigenstates are stable, new nonlinearities will be involved, leading to the existence of new locking tongues. As far as possible, these tongues will be analytically studied, using some approximations. In every case, a numerical simulation of Eqs. (26) leads to the rigorous result.

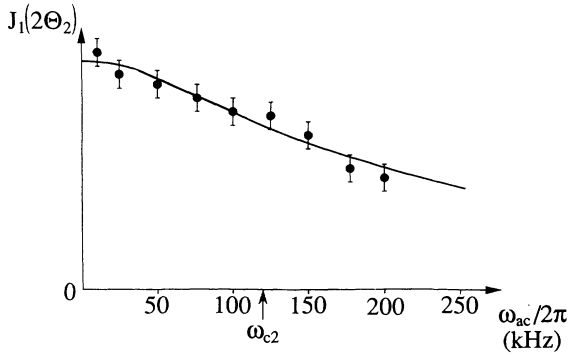

FIG. 12. Response of the polarization to an ac magnetic field in the case of two stable eigenstates. $J_1(2\Theta_2)$, proportional to the modulation of the intensity observed through the polarizer, is represented versus the frequency of the ac magnetic field (full line: theory; dots: experiment).

As already stated, the atomic parameter a (tens of MHz) is large compared to the typical frequencies (hundreds of kHz) of our system. Thus, in (26b), χ will respond almost instantaneously to a variation of θ. We can then state that $\dot{\chi}=0$, leading to

$$\dot{\theta}=-\frac{[(c/2L)\Delta\phi_{xy}]^2}{a}\sin(4\theta)+\frac{k_d}{a}\frac{c}{2L}\Delta\phi_{xy}\sin(2\theta)+\gamma[B_{dc}+B_{ac}\cos(\omega_{ac}t)]\ . \tag{34}$$

If the laser is tuned to line center, $k_d=0$ [28]. Thus (34) becomes similar to (3), except that $\sin(2\theta)$ is replaced by $\sin(4\theta)$ in the first locking term, because there are two times more wells in the potential. The arguments used to understand the lockings in Sec. III can then be used, but with two stable eigenstates instead of only one. Thus the locking will follow the law $\omega_{ac}\approx 2\omega_{dc}/n$. But, when the laser is not tuned to line center, $k_d\neq 0$, and the term with $\sin(2\theta)$ will play a significant role. It leads to the existence of locking tongues following the law $\omega_{ac}\approx\omega_{dc}/n$. The combination of these two laws will then produce some small lockings like $\frac{3}{5}, \frac{3}{7}, \ldots$. These small lockings follow the Farey hierarchy [4]. Once again, although the dynamics is more complicated than in the case of a loss anisotropy (only one stable eigenstate), no chaos can be expected, because χ is also adiabatically eliminated, like the atomic variables.

B. Experimental verification

The same laser is used as previously, except that plate 1 is employed only to compensate the residual loss anisotropies. Plate 2 is carefully stressed, in order to produce the desired phase anisotropy.

1. *ac magnetic field alone*

The experiment is performed in the same way as for one stable eigenstate. The amplitude of the response of the polarization is displayed experimentally by the dots in Fig. 12, for a motion around $\theta=0$, one of the stable eigenstates. The theoretical curve is in full line and

comes from (30), with $\Delta\Phi_{xy}=0.5°$. It leads to $\omega_{c2}/2\pi=122$ kHz. This curve is only valid for weak ac magnetic field. This behavior shows the importance of considering the response of the polarization to an ac magnetic field, as with one stable eigenstate. But, in addition, one must notice that for two stable eigenstates, this behavior could also occur around $\theta=\pi/2$, because this position correspond to a stable eigenstate too.

2. *Superimposed ac and dc magnetic fields*

With an extra dc magnetic field $B_{dc}=1.1$ G, which produces $\omega_{dc}/2\pi=126$ kHz, some new lockings occur, as shown in Fig. 13(a) [theoretical tongues obtained by simulating Eqs. (26)] and Fig. 13(b) (experiment). The Faraday rotation coefficient is $\gamma=443\,000$ rad s^{-1}. The phase anisotropy is $\Delta\Phi_{xy}=0.61°$. The other parameters used for the simulation are $a=3\times10^7$ s^{-1} and $L=0.545$ m. The locking tongues with winding numbers $2/n$ are clearly seen. Since the detuning of the cavity from line center is $\Delta\nu=-10$ MHz, leading to $k_d=-10^6$ s^{-1}, other tongues appear. Moreover, the main tongues, following the ratio $2/n$, are different from those of Sec. III, because of the term containing $\sin(2\theta)$ in Eq. (34), which prevents the arguments of Sec. III from being exact. Nevertheless, the width of the tongues varies almost periodically with B_{ac}. The new tongues following the Farey hierarchy can be studied more precisely thanks to the bifurcation diagrams of Fig. 14 with $B_{ac}=5.57$ G. Figure 14(a) is theoretical, and Fig. 14(b) is experimental. A p/q tongue

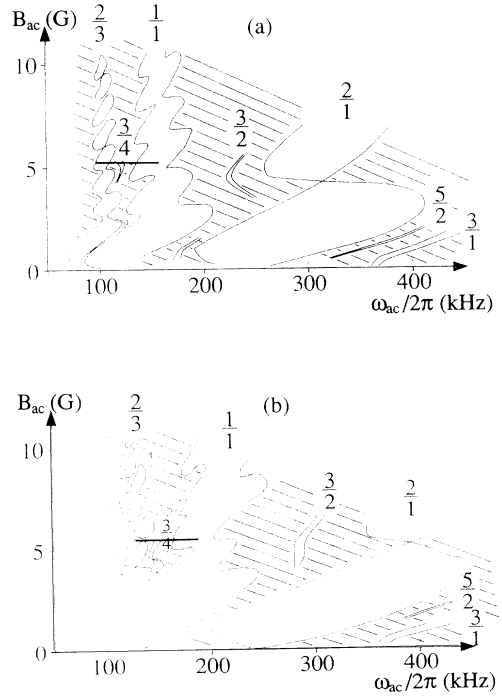

FIG. 13. Theoretical (a) and experimental (b) locking tongues in the plane $(\omega_{ac}/2\pi, B_{ac})$ for two stable eigenstates. The hatched domains correspond to a motion with unlocked frequencies (quasiperiodicity). The line shows the location of the bifurcation diagrams of Fig. 14.

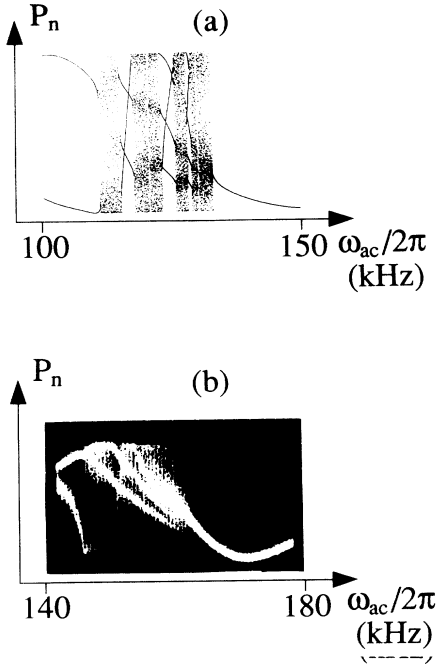

FIG. 14. Theoretical (a) and experimental (b) bifurcation diagrams for two stable eigenstates, between $\frac{2}{3}$ and $\frac{1}{1}$ tongues. (a) is adjusted at $B_{ac}=5.3$ G. (b) is measured with $B_{ac}=5.57$ G.

$(p\omega_{dc}$ locks with $q\omega_{ac})$ is characterized by p lines. We notice the following series: two lines, many points, three lines, many points, four lines, etc. This corresponds to $\frac{2}{3}$, quasiperiodicity, $\frac{3}{4}$, quasiperiodicity, $\frac{4}{5}$, etc., corresponding to the horizontal line of Fig. 13. In Figs. 15(a)–15(d), the same tongues are analyzed by measuring the spectrum of the signal in particular regions, with $B_{ac}=5.57$ G. The spectrum in Fig. 15(a), with $\omega_{ac}/2\pi=145$ kHz, corresponds to the tongue $\frac{2}{3}$, and has a peak at $(\omega_{ac}/2\pi)/2$. In Fig. 15(b), $\omega_{ac}/2\pi=148$ kHz, and the regime is quasiperiodic. In Fig. 15(c), $\omega_{ac}/2\pi=151.5$ kHz, and the tongue $\frac{3}{4}$ gives a peak at $(\omega_{ac}/2\pi)/3$. In Fig.

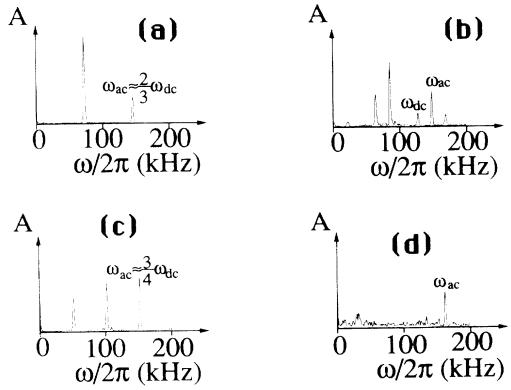

FIG. 15. Experimental spectra for two stable eigenstates at four different points in the plane $(\omega_{ac}/2\pi, B_{ac})$ in Fig. 13(b). $B_{ac}=5.57$ G. (a) $\omega_{ac}/2\pi=145$ kHz; (b) $\omega_{ac}/2\pi=148$ kHz; (c) $\omega_{ac}/2\pi=151.5$ kHz; (d) $\omega_{ac}/2\pi=162$ kHz. These spectra correspond to the bifurcation diagram of Fig. 14(b).

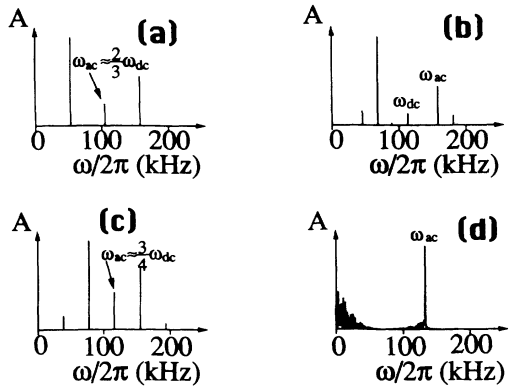

FIG. 16. Theoretical spectra corresponding to Fig. 15. These spectra correspond to the bifurcation diagram of Fig. 14(a).

15(d), $\omega_{ac}/2\pi=162$ kHz, and the regime is quasiperiodic, with many peaks. The corresponding theoretical spectra are given in Figs. 16(a)–16(d).

In the case of two stable eigenstates, new *quasitwisted Arnold tongues* are encountered. The first ones correspond to the fact that there are two times more eigenstates. Thus the lockings follow the law $\omega_{ac}\approx 2\omega_{dc}/n$, instead of $\omega_{ac}\approx\omega_{dc}/n$. Moreover, other small tongues appear, which follow the Farey hierarchy, but *no chaos* occurs, even if the laser is detuned. Good agreement is observed between theory and experiment, and the lockings are also physically understood.

V. CONCLUSION

In conclusion, we have shown the influence of the number of stable eigenstates of a vectorial laser on the nonlinear dynamic behavior of the polarization of such a laser subjected either to a longitudinal ac magnetic field at frequency ω_{ac} or to the simultaneous action of longitudinal ac and dc magnetic fields. First, the concept of response time of the polarization to a weak sinusoidal forcing has been put into evidence. This leads to the existence of a cutoff frequency, experimentally isolated, for the amplitude of the response of the laser, due to cavity effects. But, in spite of this cutoff frequency, these cavity effects permit us to enhance appreciably the amplitude of the vibration of the polarization, compared with a single-pass experiment. Second, we have exhaustively studied the lockings between the rotational and vibrational motions of the polarization created by a dc and an ac magnetic field, respectively. In particular, we have shown the existence of the *twisted Arnold tongues* (one stable eigenstate) and the *quasitwisted Arnold tongues* (two stable eigenstates), also previously predicted in the theoretical studies on the dissipative standardlike map [30], and the possible ratios of the locked frequencies, depending on the number of stable eigenstates. We have shown that such inertialess systems as laser polarization vectors constitute an ideal tool for the observation of twisted Arnold tongues to high-order narrowings. The rotational angular frequency ω_{dc} has been shown to lock with $n\omega_{ac}$ in the case of *one* stable eigenstate and with $(n/2)\omega_{ac}$ in the case of *two* stable eigenstates. These results have been physically interpreted. Moreover, no chaos is observed in these systems, due to the adiabatic elimination of one of the variables (intensity in one case, ellipticity in the other), but the observed dynamics remains typical of each case. This absence of chaos is also explained by the *noncoalescence* of our twisted Arnold tongues, but nevertheless, is not due to the existence of a cutoff frequency, which is associated with an extra nonlinearity. In every case, good agreement is obtained between experiment and theory. Besides, we have experimentally checked that the laser exhibits the same kind of behaviors in the case of a nonweak atomic coupling $J=1\rightarrow J=1$ transition. In particular, it does not exhibit vectorial chaos either. However, in numerical simulation, the model for the case of two stable eigenstates could exhibit chaos, but only for *unrealistic* values of the parameters which forbid adiabatic elimination of the ellipticity. One can thus meaningfully compare our system to such mechanical vectorial systems as a compass needle up to a certain point. Indeed, neither the intensity nor the ellipticity of our system can play the role of the inertia of mechanical systems. This feature is particularly interesting in the case of the laser magnetometer [13]. Indeed, this device which transforms a weak dc longitudinal magnetic field into a frequency cannot have an erratic behavior. Moreover, since it exhibits a small locking region due to residual anisotropies, this locking region must consequently be circumvented thanks to an ac magnetic field. Our work provides the clues necessary for the choice of the dithering parameters, adapted to each typical locking regime ($1/n$ or $2/n$). Moreover, this shows that vectorial bistable laser systems used for optical logic, which are two-stable-eigenstate devices [31], cannot exhibit vectorial chaos, under usual conditions. This study could also throw light on the physical understanding of systems governed by a forced Adler equation, for example, a laser gyro.

ACKNOWLEDGMENTS

This research was supported by the "Centre National de la Recherche Scientifique," the "Direction des Recherches, Etudes et Techniques," the "pôle optique et optoélectronique de la Formation des Ingénieurs par la Recherche Technologique," and the "Conseil Régional de Bretagne." The Laboratoire d'Electronique Quantique-Physique des Lasers is "Unité de Recherche Associée au CNRS No. 1202" and the Laboratoire de Spectroscopie Hertzienne is "URA au CNRS No. 249."

[1] V. Croquette and C. Poitou, J. Phys. (Paris) Lett. **42**, L537 (1981).
[2] M. J. Ballico and M. L. Sawley, Am. J. Phys. **58**, 58 (1990).
[3] M. H. Jensen, P. Bak, and T. Bohr, Phys. Rev. A **30**, 1960 (1984); T. Bohr, P. Bak, and M. H. Jensen, *ibid.* **30**, 1970 (1984); P. Bak, Phys. Today **39** (12), 38 (1986); J. A. Glazier and A. Libchaber, IEEE Trans. Circ. Syst. **35**, 790 (1988).

[4] P. Bergé, Y. Pomeau, and C. Vidal, *Order Within Chaos* (Wiley, New York, 1986).

[5] F. T. Arecchi, R. Meucci, G. Puccioni, and J. Tredicce, Phys. Rev. Lett. **49**, 1217 (1982); T. Midavaine, D. Dangoisse, and P. Glorieux, *ibid.* **55**, 1989 (1985); in *Instabilities in Active Optical Media,* edited by N. B. Abraham, L. A. Lugiato, and L. M. Narducci, special issue of J. Opt. Soc. Am. B **2** (1) (1985); in *Nonlinear Dynamics of Lasers,* edited by D. K. Bandy, A. N. Oraevsky, and J. R. Tredicce, special issue of J. Opt. Soc. Am. B **5** (5) (1988); and (unpublished); J. Sacher, D. Baums, P. Panknin, W. Elsässer, and E. O. Göbel, Phys. Rev. A **45**, 1893 (1992).

[6] C. O. Weiss, N. B. Abraham, and U. Hübner, Phys. Rev. Lett. **61**, 1587 (1988).

[7] A. Le Floch, G. Ropars, J.-M. Lenormand, and R. Le Naour, Phys. Rev. Lett. **52**, 918 (1984).

[8] G. P. Puccioni, G. L. Lippi, N. B. Abraham, and F. T. Arecchi, Opt. Commun. **72**, 361 (1989).

[9] G. P. Puccioni, M. V. Tratnik, J. E. Sipe, and G. L. Oppo, Opt. Lett. **12**, 242 (1987).

[10] A. P. Voitovich, L. P. Svirina, and V. N. Severikov, Opt. Commun. **80**, 435 (1991); S. Grossmann and D. Yao, Z. Phys. B **80**, 439 (1990).

[11] J.-C. Cotteverte, F. Bretenaker, and A. Le Floch, Opt. Commun. **79**, 321 (1990).

[12] H. Statz, R. Paananen, and G. F. Koster, J. Appl. Phys. **33**, 2319 (1962).

[13] F. Bretenaker, B. Lépine, J.-C. Cotteverte, and A. Le Floch, Phys. Rev. Lett. **69**, 909 (1992).

[14] M. Born and E. Wolf, *Principles of Optics* (Pergamon, New York, 1959).

[15] P. Glorieux and A. Le Floch, Opt. Commun. **79**, 229 (1990).

[16] A. Le Floch and R. Le Naour, Phys. Rev. A **4**, 290 (1971).

[17] F. Bretenaker, A. Le Floch, J. Davit, and J.-M. Chiquier, IEEE J. Quantum Electron. **QE-28**, 348 (1992).

[18] J.-C. Cotteverte, F. Bretenaker, and A. Le Floch, Opt. Lett. **16**, 572 (1991); in *Nonlinear Dynamics and Quantum Phenomena in Optical Systems,* edited by R. Vilaseca and R. Corbalàn, Vol. 55 (Springer-Verlag, Berlin, 1991), p. 206.

[19] M. Sargent III, M. O. Scully, and W. E. Lamb, Jr., *Laser Physics* (Addison-Wesley, Reading, MA, 1974).

[20] V. De Giorgio and M. O. Scully, Phys. Rev. A **2**, 1170 (1970).

[21] R. Adler, Proc. IRE **34**, 351 (1946).

[22] W. Culshaw and J. Kannelaud, Phys. Rev. A **136**, 1209 (1964).

[23] H. de Lang and G. Bouwhuis, Phys. Lett. **19**, 481 (1965).

[24] L. Schwartz, *Méthodes Mathématiques Pour les Sciences Physiques* (Hermann, Paris, 1965).

[25] Y. Rocard, *Théorie des Oscillateurs* (Revue Scientifique, Paris, 1941).

[26] W. W. Chow, J. Gea-Banacloche, L. M. Pedrotti, V. E. Sanders, W. Schleich, and M. O. Scully, Rev. Mod. Phys. **57**, 61 (1985).

[27] J.-C. Cotteverte, F. Bretenaker, and A. Le Floch, Appl. Opt. **30**, 305 (1991).

[28] W. Van Haeringen, Phys. Rev. **158**, 256 (1967).

[29] M. Sargent III, W. E. Lamb, Jr., and R. L. Fork, Phys. Rev. **164**, 436 (1967); **164**, 450 (1967); W. J. Tomlinson and R. L. Fork, *ibid.* **164**, 466 (1967).

[30] S.-Y. Kim and B. Hu, Phys. Rev. A **44**, 934 (1991).

[31] G. Ropars, A. Le Floch, and R. Le Naour, Europhys. Lett. **3**, 695 (1987); Phys. Rev. A **46**, 623 (1992).

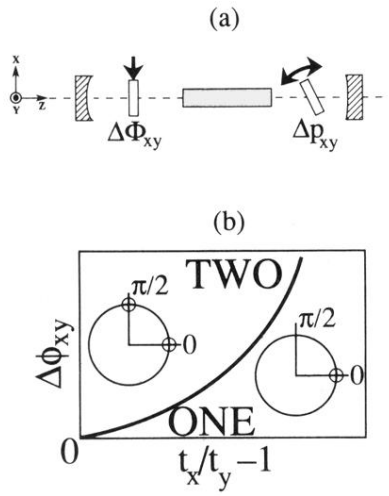

FIG. 1. (a) Laser containing loss (Δp_{xy}) and phase ($\Delta\Phi_{xy}$) anisotropies. (b) One-eigenstate and two-eigenstate stability domains. The diagram is displayed in the plane of phase anisotropies versus loss anisotropies. In each domain, the corresponding potential wells are represented. The abscissa and ordinate axes correspond to pure loss and phase anisotropies, respectively.

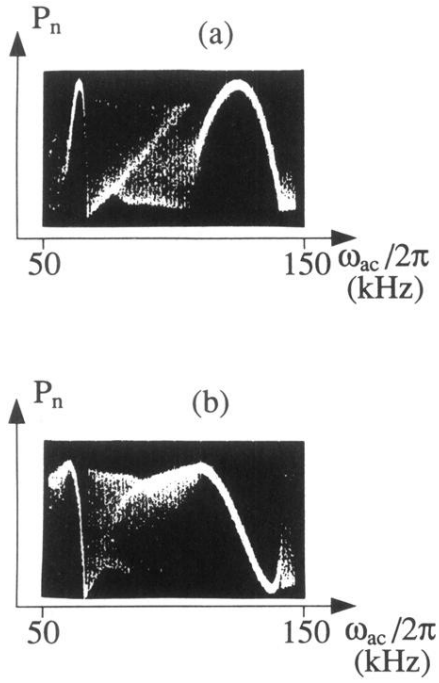

FIG. 10. Experimental bifurcation diagrams for one stable eigenstate, and for two different positions of the polarizer: (a) $\theta_p = 0$; (b) $\theta_p = 45°$. $B_{ac} = 0.3$ G.

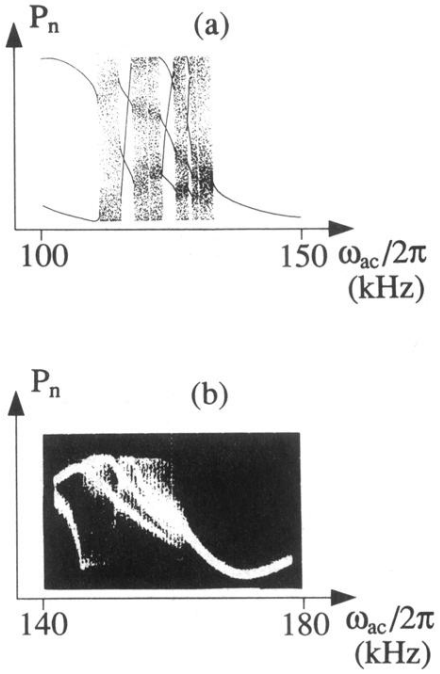

FIG. 14. Theoretical (a) and experimental (b) bifurcation diagrams for two stable eigenstates, between $\frac{2}{3}$ and $\frac{1}{1}$ tongues. (a) is adjusted at $B_{ac}=5.3$ G. (b) is measured with $B_{ac}=5.57$ G.

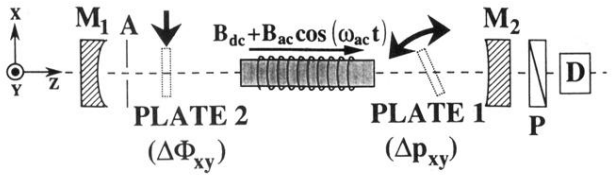

FIG. 7. Experimental setup used to observe the behavior of the polarization with an ac magnetic field alone ($B_{dc}=0$), or superimposed onto a dc magnetic field. Plate 1 produces the loss anisotropy used in the case of only one stable eigenstate, and plate 2 produces the phase anisotropy used in the case of two stable eigenstates.

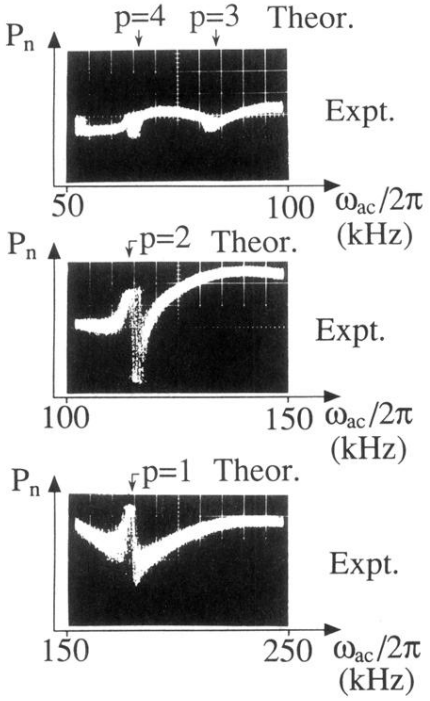

FIG. 8. Experimental signal sampled at $\omega_{ac}/2\pi$ for several values of p. Between the T_{ac}-periodical zones where θ_0 is stable, some nonperiodical zones exist, where the system hesitates between $\theta_0=0$ and $\pi/2$.